New Journal of Physics
The open-access journal for physics

Reduction and degradation of amyloid aggregates by a pulsed radio-frequency cold atmospheric plasma jet

D L Bayliss[1], J L Walsh[1], G Shama[2], F Iza[1] and M G Kong[1,3]

[1] Department of Electronic and Electrical Engineering, Loughborough University, Leicestershire LE11 3TU, UK

[2] Department of Chemical Engineering, Loughborough University, Leicestershire LE11 3TU, UK

E-mail: m.g.kong@lboro.ac.uk

New Journal of Physics **11** (2009) 115024 (16pp)
Received 24 July 2009
Published 26 November 2009
Online at http://www.njp.org/
doi:10.1088/1367-2630/11/11/115024

Abstract. Surface-borne amyloid aggregates with mature fibrils are used as a non-infectious prion model to evaluate cold atmospheric plasmas (CAPs) as a prion inactivation strategy. Using a helium–oxygen CAP jet with pulsed radio-frequency (RF) excitation, amyloid aggregates deposited on freshly cleaved mica discs are reduced substantially leaving only a few spherical fragments of sub-micrometer sizes in areas directly treated by the CAP jet. Outside the light-emitting part of the CAP jet, plasma treatment results in a 'skeleton' of much reduced amyloid stacks with clear evidence of fibril fragmentation. Analysis of possible plasma species and the physical configuration of the jet–sample interaction suggests that the skeleton structures observed are unlikely to have arisen as a result of physical forces of detachment, but instead by progressive diffusion of oxidizing plasma species into porous amyloid aggregates. Composition of chemical bonds of this reduced amyloid sample is very different from that of intact amyloid aggregates. These suggest the possibility of on-site degradation by CAP treatment with little possibility of spreading contamination elsewhere, thus offering a new reaction chemistry route to protein infectivity control with desirable implications for the practical implementation of CAP-based sterilization systems.

[3] Author to whom any correspondence should be addressed.

Contents

1. Introduction

Cold atmospheric plasmas (CAPs) provide a rich source of reaction chemistry with abundant charged particles, radicals and excited species, and ultraviolet (UV) photons, each of which are known to interact strongly with biomolecules, cells and tissues [1, 2]. Some plasma species such as oxygen atoms and OH radicals are known to inactivate bacterial cells [3, 4], while others such as nitric oxides are found to stimulate proliferation of mammalian cells in a wound healing context [5, 6]. Fundamentally, CAPs can be tailored to influence cell functions from 'plasma-mediated kill' to 'plasma-mediated heal'. Their implications for medicine and healthcare are reflected in the current intense and rapidly expanding research activities in medical sterilization [1]–[4], wound care [5, 6], cancer therapies [7]–[10], dentistry [11]–[14] and food decontamination [15]–[18]. Together, these research areas constitute the vast majority of the present focus of plasma medicine.

Medical sterilization was the first topic of research in the history of plasma medicine [1], and today it still represents the area with the greatest level of research activity. Much of the published work on CAP application to medical sterilization has focused on microbial inactivation [1]–[4], [19]–[31]. However, protein and tissue contamination of surgical instruments are common following surgery [32]. Conventional sterilization procedures such as autoclaving and/or ethylene oxide vapour may suffer compromised efficacy because tissue residues may evade destruction when present in the lumens of surgical instruments and medical devices (e.g. endoscopes) [33]. However, the greatest challenge to conventional sterilization strategies is contamination by prions—misfolded proteins that defy current commercial decontamination procedures [34]. Implicated in transmissible spongiform encephalopathy (TSE), in particular variant Creutzfeldt–Jakob disease (vCJD) in humans and bovine spongiform encephalopathy (BSE) in cattle, prions are considerably more resistant to external stresses than bacteria, viruses and fungi [35]. Prion contamination is the ultimate challenge in medical sterilization, and at present the only viable option for preventing prion contamination during surgery is to adopt a policy of single-use surgical instruments. Low-temperature gas plasmas generated both at reduced pressure [36]–[40] and atmospheric pressure [41, 42] represent one of very few potential pipeline solutions.

The challenge of prion contamination is not only the extreme resistance of prion agents to many physical and chemical decontaminants but also the complexity of their infectivity in mammalian hosts. Recent studies have revealed considerable variation in animal survival as estimated using a number of different bioassay models when subjected to the same prion contamination [43] and this raises questions over the suitability of many of the existing animal models. Whereas the need for more appropriate animal models is clear, it will take some time before they become available for decontamination studies. Given this and the current limited understanding of plasma–prion interactions [36]–[42], it is both important and logical to address fundamental questions of responses to CAP treatment of different prions and prion-like proteins. Results from experiments aimed at answering such questions could form a knowledge base from which to gain greater confidence in plasma inactivation of prion proteins including vCJD agents. It is with the above considerations that we consider amyloid proteins, which have a very similarly misfolded β-sheet structure to prions [44], as an appropriate non-infectious model of prion structure to plasma treatment. In particular, amyloid fibrils and prions are both proteinaceous aggregates that are based on a unique form of polypeptide configuration, namely the cross-β structure [45]. Effective plasma inactivation of amyloid fibrils would offer further confidence in the viability of plasma inactivation of human prions.

This study employs a pulsed radio-frequency (RF) CAP jet to treat amyloid aggregates deposited on freshly cleaved mica discs. The pulsed RF CAP jet is characterized using electrical measurements, gas temperature determination and optical emission spectroscopy. Atomic force microscopy (AFM) is used to characterize the growth of amyloid fibrils on mica discs and the impact of CAP treatment. These results suggest a neutral radical-based mechanism for amyloid aggregates reduction, particularly in locations remote from the light-emitting part of the plasma jet. This reduction mechanism may be the result of the diffusion of reactive oxygen species into the porous amyloid aggregates and their progressive fragmentation and degradation of amyloid fibrils. Finally, x-ray photoelectron spectroscopy (XPS) is used to provide additional support for possible mechanisms of removal of amyloid aggregates.

2. Methods and materials

2.1. CAP sources

For surgical instrument decontamination, CAP jets are more appropriate than the usual parallel-plate configuration. When used to treat three-dimensional (3D) objects, parallel-plate electrode configurations sometimes result in constricted plasmas making them unattractive for medical sterilization, particularly for atmospheric plasmas that are prone to glow-to-arc transition. On the other hand, CAP jets are more resistant to glow-to-arc transition due to a spatial separation of plasma generation from plasma processing [46] and they can be scaled up in large-scale jet arrays [47, 48] in anticipation of their eventual use for batched decontamination of surgical instruments. With appropriate electrode design and power electronics, CAP arrays have been shown to offer a robust and reasonably uniform treatment of surgical instruments, for example tissue forceps [48]. Therefore CAP jets and jet arrays represent a more realistic strategy for treatment of 3D objects than CAP sustained between parallel-plate electrodes.

For this study, we employed a linear-field CAP jet of which the electric field was predominately in parallel to the gas flow field [49]. Such an electrode structure has recently been shown to enable a stronger plasma plume in the downstream region where the sample is

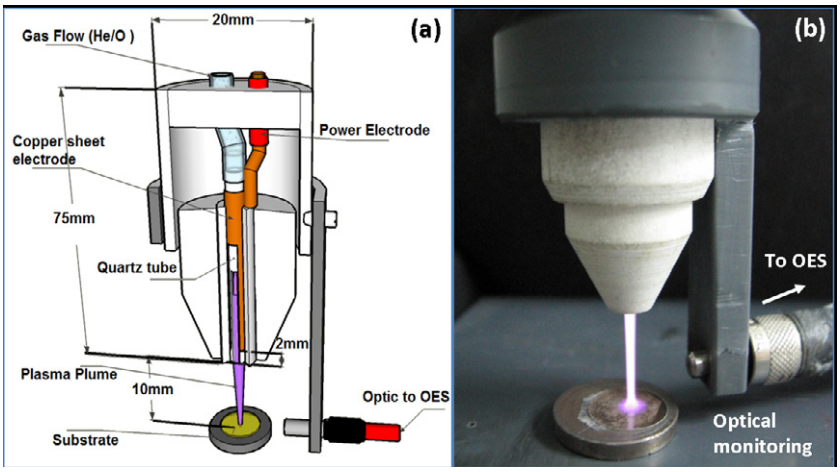

Figure 1. A low-temperature atmospheric plasma jet in helium–oxygen flow with (a) a schematic showing its main components and (b) a digital image of the CAP jet treating a stainless steel plate.

usually placed, compared to the cross-field electrode configuration where the electric field is perpendicular to the gas flow field [49]. Figure 1(a) shows the schematic of the atmospheric plasma jet. For this study, the jet plasma configuration consisted of a quartz tube measuring 75 mm in length with a 2 mm inner diameter and 3 mm outer diameter. A 70 mm wide metallic electrode was wrapped tightly around the quartz tube at a distance of 2 mm from the tube nozzle. A second grounded metallic electrode was placed 1 cm downstream from the nozzle, and this was also used as the sample holder. An optical monitoring unit was mounted onto the jet housing unit so that its position from the plasma jet plume was kept constant to eliminate variations due to repeated assembling and dismounting of the apparatus. The tip of the optical probe was 6 mm vertically from the jet nozzle and horizontally 6 mm from the plasma jet. An MKS mass flow controller was employed to provide a constant helium flow (99.996% purity) of 10 standard litres per minute (slm) mixed with oxygen at 50 standard cubic centimetres per minute (sccm). The oxygen to helium ratio was 0.5%, chosen because it was found to be most effective against both bovine serum albumin (purified protein) [41, 42] and microbes in our previous studies [3, 4, 50]. Figure 1(b) shows a helium plasma jet with a discharge diameter of approaching 2 mm and a discharge volume of approximately 157 mm^3.

The choice of the excitation frequency is important as it affects significantly the dynamics and kinetics of CAPs, both for dielectric-barrier discharges [51] and for RF atmospheric glow discharges [52]. Given the ultimate aim of inactivating resistant prions, it is important to produce an intense plasma in order to maximize its destructive effects. High excitation frequencies produce more intense plasmas, but high-frequency plasmas tend to have high gas temperature thus restricting their use for biomedical applications [53]–[55]. One technique to achieve intense plasmas at low gas temperatures is to pulse-modulate the RF excitation [56]–[59]. To this end, we employed a main RF excitation at 3.9 MHz and its modulation at 25 kHz with a duty cycle of 25%. This pulsed RF modulation reduced the gas temperature to 55 °C with atomic emission intensity at 777 nm approaching 0.3 $\mu W\,cm^{-2}\,nm^{-1}$ (see below for further discussion).

2.2. Plasma condition monitoring

For electrical measurements, a Tektronix P6015A 1000 : 1 75 MHz high voltage probe was connected to the wrapped electrode and a Pearson 2877 1 V/1 A 200 MHz current monitor was inserted between the ground electrode and the grounding point. A Tektronix DPO4104 oscilloscope was employed to record current and voltage signals, with its 1 GHz bandwidth and 10 mega-sample record length making it an ideal choice for recording many cycles of the applied voltage. For optical diagnostics, an optical fibre of 600 μm in diameter was positioned inside the optical monitoring unit at 6 mm below the tube nozzle and fixed radially 6 mm from the axis of the plasma plume. Emission spectra were obtained using an Andor Shamrock SR-303i spectrometer with a focal length of 303 mm. Detailed spectra were acquired using a 2400 lines mm^{-1} grating providing a 0.01 nm spectral resolution, overview spectra were obtained using a 600 lines mm^{-1} grating providing a 0.13 nm spectral resolution. Absolute emission intensity calibration was performed with an Ocean Optics LS-1-CAL NIST traceable white light source, providing absolute intensity values from 350 to 900 nm. All optical spectroscopic measurements were conducted with the optical monitoring unit, and the fixed distance of the latter to the plasma jet was important to ensure reproducibility from one experiment to the next and to enable comparison to future independent experiments. This is important as atmospheric plasmas are known to be susceptible to changes in environmental conditions. Gas temperature was measured at the sample point using temperature strips, and its dependence on input RF power was confirmed by rotational temperature measured from the nitrogen monopositive ion N_2^+ first negative system ($B^2\Sigma_u^+,\ v = 0 \rightarrow X^2\Sigma_g^+,\ v' = 0$, 388–392 nm).

2.3. Amyloid fibre growth and preparation

Amyloid $\beta_{1\text{-}42}$ fibres were prepared and grown as described in the literature [60]. Lyophilized peptide was treated in 1,1,1,3,3,3-Hexafluoro-2-Propanol (HFIP). Each vial of peptide was diluted in 100% HFIP to 1 mM and the clear solution containing the dissolved peptide was then aliquoted in micro centrifuge tubes. The HFIP was allowed to evaporate in a fume hood and the resulting clear peptide films were dried under vacuum and stored desiccated at −20 °C.

For fibre growth, the protein films was resuspended to form a 5 mM solution in anhydrous dimethyl sulfoxide (Me_2SO) by pipette mixing followed by bath sonication for 10 min. The 5 mM solution was diluted to 100 μM in 10 mM HCl, immediately vortexed for 30 s, and incubated at 37 °C. Samples were removed at several time intervals for amyloid fibre growth assessment. Mica discs of 9.9 mm in diameter (Agar Scientific) were attached to steel discs with double-sided tape for ease of cleavage. Amyloid suspension (30 μl) was deposited onto freshly cleaved mica and incubated at room temperature for 5 min, rinsed with 0.02 μm of filtered deionized water (Anotop 10), and blown dry with tetrafluroethane before AFM analysis. Samples prepared for plasma treatment were always grown for 24 h.

2.4. AFM

Fibres were analysed before and after plasma treatment using a Dimensions 3100 Scanning Probe Microscope (Veeco Instruments) in the tapping mode. A single-crystal silicon microcantilever was used with a resonant frequency of 350 kHz and 42 N m^{-1} spring constant model. Images were obtained using scan rates of 1 Hz.

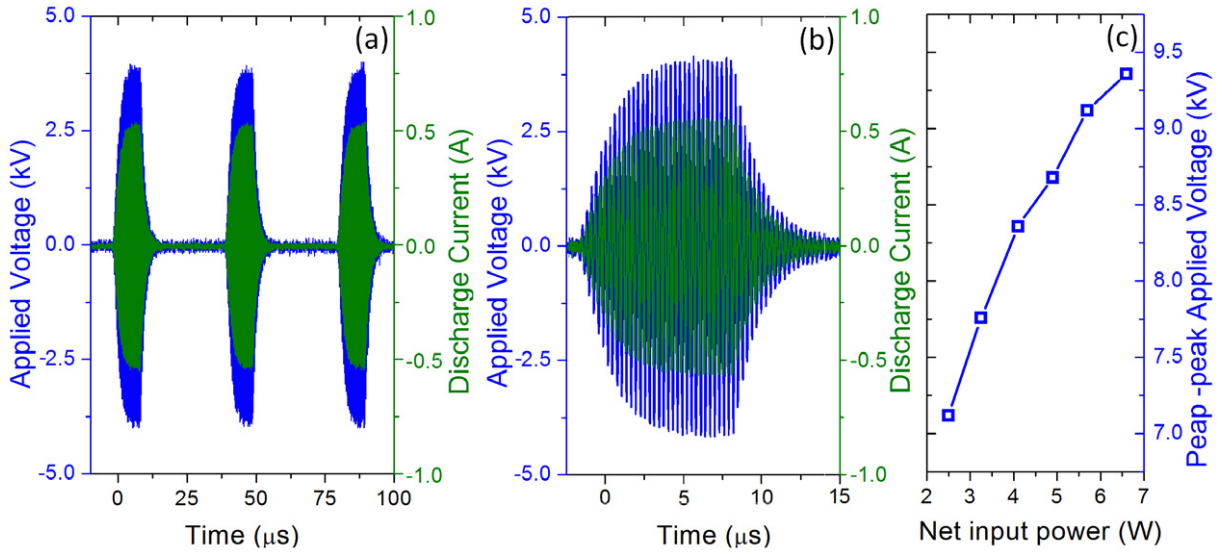

Figure 2. Electrical characteristics of the pulsed RF CAP jet with (a) voltage and current traces over three modulation cycles; (b) voltage and current over one power-on phase; and (c) RF power dependence of the applied voltage.

2.5. XPS analysis

XPS analysis was performed using a VG Escalab MK machine. Its x-ray source was ALK alpha radiation running at 8 kV 20 mA and 160 W non-monochromated. The analysis diameter was about 2 mm with a normal to surface sample electron emission angle.

2.6. CAP jet treatment

The distance from nozzle tip to mica surface was fixed at 10 mm. Plasma-treated amyloid was achieved using a net input RF power of 4 W at a peak-to-peak voltage of 8.36 kV and a peak-to-peak current of 2.196 A. Control samples were obtained by flowing gas without plasma for 5 min, heating the samples to 80 °C for 5 min with a hotplate, and a combination of the two. Plasma gas temperatures were always below 55 °C, and so the choice of 80 °C was to provide a greater thermal challenge to the surface-borne amyloid aggregates.

3. Results and discussion

Figure 2 shows electrical characteristics of the pulsed RF jet in a 10 slm atmospheric helium–oxygen flow (O_2/He = 0.5%). Pulse modulation is seen in figures 2(a) and (b) to divide the RF excitation into two distinct phases, namely the power-on and the power-off phase with 25% duty cycle for the experiments reported here. As shown in figures 2(a) and (b), one power-on phase consists of two development stages. The first stage is characterized by a gradual increase in the magnitude of rapid RF oscillations over a period of about 5 μs, and the second stage has a relatively constant RF magnitude for 5 μs. The power-on phase therefore lasts for 10 μs, equivalent to 39 RF cycles approximately at 3.9 MHz. The first stage represents the growth of the plasma jet from its ignition within the electrode unit to its reach at the ground

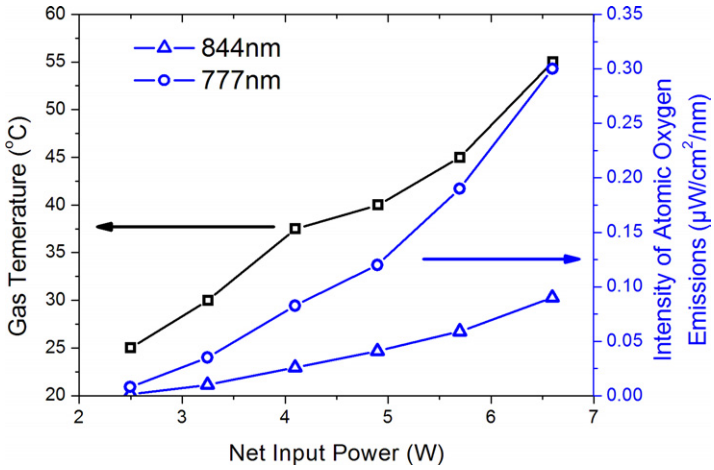

Figure 3. Gas temperature (black) and optical emission intensities at 777 and 845 nm (blue).

electrode, whereas the second stage represents a steady-state of the plasma jet. On the other hand, the power-off phase starts with a 7 μs period of gradual decay (or about 27 RF cycles) and finishes with a 23 μs period of a near-zero RF amplitude. The total duration of the power-off phase is therefore 30 μs, confirming a duty cycle at 25%. The gradual decay period represents a forced plasma quenching process by a reducing applied voltage, and the following period of near-zero RF amplitude represents a quenched plasma though some residual charges may remain in the jet structure. In figure 2(c), the applied voltage is shown to increase monotonically with net input power. With a net input power of 2–4 W, the power–voltage relationship is roughly linear. However, at larger input RF power, the value of the applied voltage becomes proportionally smaller. This suggests a progressively more resistive plasma at large input RF power. For treatment of the amyloid aggregates reported here, the RF power was fixed at 4 W and the plasma jet was capacitive with the voltage–current phase angle close to 90° in the steady-state of the power-on phase. It is worth mentioning that 4 W is equivalent to 25.5 W cm^{-3} for our CAP jet, lower than typical dissipated power in conventional continuous-wave RF atmospheric glow discharges [61].

Figure 3 shows RF power dependence of gas temperature and two atomic oxygen emission intensities at 777 and 845 nm, respectively. Gas temperature was measured at the plasma contact point on the sample surface using a temperature stripe, and was confirmed for power dependence using rotational temperature measured from the nitrogen ion N_2^+ first negative system ($B^2\Sigma_u^+$, $v = 0 \rightarrow X^2\Sigma_g^+$, $v' = 0$, 388–292 nm). Given that the pulsed RF plasma jet was intended to provide oxygen chemistry with 0.5% oxygen admixture in the background helium flow, the two excited atomic oxygen lines at 777 and 845 nm were used as an indicator for monitoring purposes. It is evident that gas temperature was below 55 °C for all experimental conditions with net input RF power up to 6.6 W. More specifically under the plasma conditions considered here, the RF power was fixed at 4 W and according to figure 3 the gas temperature was about 37 °C. For all amyloid experiments reported here, the plasma treatment was no more than 8 s in duration and as such it was very unlikely that the amyloid sample would experience temperatures markedly above ambient. In other words, the plasma effects were most likely to be non-thermal. The absolute emission intensity reaches 0.30 and 0.09 μW cm^{-2} nm^{-1} at 6.6 W

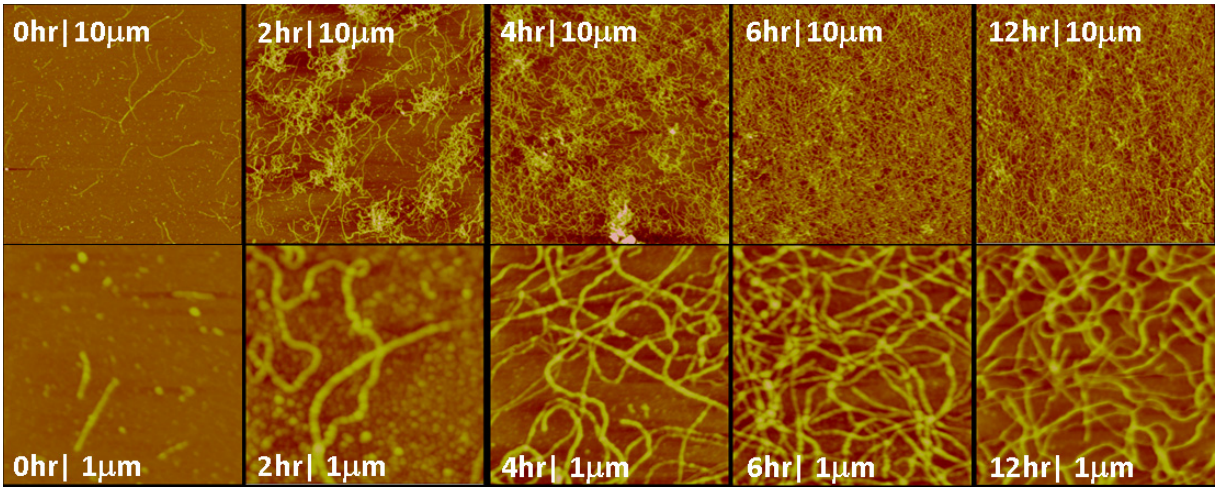

Figure 4. Growth of amyloid aggregates over a course of 12 h with the top row showing AFM images on a scale of 10 μm and the bottom row on a scale of 1 μm. Fibrils are clearly visible.

for 777 and 845 nm, respectively. At 4 W of input RF power, the emission intensity is 0.076 and 0.027 μW cm^{-2} nm^{-1}, respectively, at 777 and 845 nm.

Figure 4 shows AFM images of amyloid samples growing over a course of 12 h on mica discs. Some fibrils are visible in the sample at 0 h and these grow into substantial aggregates after 2 h. At 4 h, clear stacking of fibrils is evident. It is known that amyloid fibre formation starts with native-state monomers and first enters a lag phase [62]. During the lag phase, they can evolve into complete denatured-state monomers and then to unstructured aggregates before becoming amyloid seeds. An alternative route to amyloid seeds is through native-state dimers and then small amyloidogenic oligomers. Amyloid seeds mark the beginning of the growth phase in which amyloid seeds undergo elongation to form filaments, the resulting amyloid filaments bundle to form protofibrils, and finally the protofibrils bundle further to become mature fibrils [62]. Mature fibrils are very strongly attached to surfaces and are difficult to remove.

Figure 5 shows AFM images of control amyloid aggregates and those with only 2 s of plasma treatment. All amyloid samples were taken after 24 h of growth, and each AFM image was taken over an area of 1 μm^2. Four controls were considered, namely an untreated sample (left in a fume hood), a sample under an unionized helium flow (i.e. no plasma) at 10 slm for 5 min, a sample heated to 80 °C in a sample holder for 5 min, and finally, a sample under the combined action of 10 slm helium flow and heating at 80 °C for 5 min. It is clear from figure 5 that these control conditions had little impact on either the topology of amyloid distribution or the appearance of amyloid fibrils. In other words, amyloid aggregates show no sign of vulnerability as a result of these physical treatments. However, with only 2 s treatment of room temperature plasma treatment at 4 W of input RF power, amyloid aggregates suffered substantial reduction with only small, roughly spherical fragments left in the central region of the treated mica disc. This substantial reduction was consistently observed in several independent experiments and at different sampling points of AFM imaging in the central area. Given the extensive stacking of amyloid fibrils at 12 h in figure 4 and their extreme resistance to

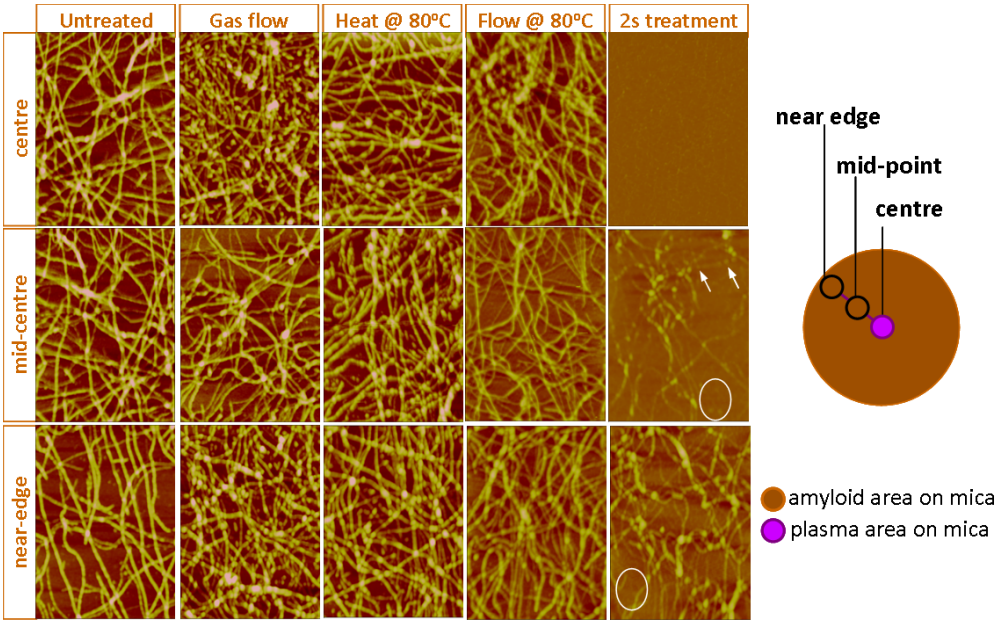

Figure 5. AFM images of amyloid aggregates obtained at the sample centre (the first row), near the mid-point along a radial line between the centre and the sample edge (the second row) and near the sample edge (the third row). The schematic on the right indicates a plasma diameter of ∼2 mm in relation to the sample diameter of 9.9 mm. Images in the first to the fourth columns are for untreated, unionized helium flow at 10 slm, heated at 80 °C, and 10 slm with heating at 80 °C, respectively. The fifth column shows results of 2 s plasma jet treatment.

heat and gas flow in figure 5, the results of plasma treatment seen in the last column of figure 5 are particularly effective.

In addition, AFM images were taken at the mid-point between the mica disc centre and the sample edge of the disc and also from a point near the sample edge. These two locations were approximately 2 and 4 mm, respectively, from the rim of the plasma diameter, and were therefore outside the reach of the light-emitting part of the plasma jet. Figure 5 suggests a clear reduction of amyloid aggregates and the reduction becomes progressively less severe towards the sample edge. At the mid-point, the fibrils are shorter and thinner with less brightness contrast than those in the control samples and there is a strong evidence of the amyloid stacks having been reduced. Some fibrils appear to have discontinuous sections (marked with arrows), and the image has regions of small blurred features (marked with a circle). In general, the fibrils featured in the image have much less defined boundaries than those of, for example, the mid-point image of the combined heat and flow case. Similar observations can also be made in the image near the sample edge, albeit to a lesser extent. These features of plasma treatment are unlikely to be the result of the action of detachment or other physical forces that might cause the break up of individual fibrils and their aggregates. In other words, it is highly unlikely that the amyloid damage outside the plasma diameter are due to simple peeling-off of the intact amyloid aggregates without fundamental modification to their chemical make-up. Instead, the evidence suggests a subtle impact of progressive diffusion of plasma agents onto the porous

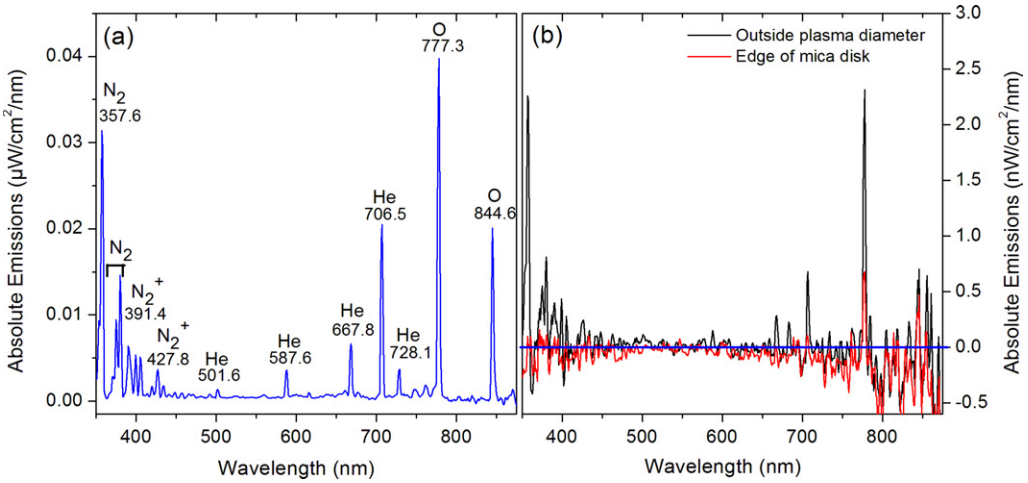

Figure 6. Absolute optical emission spectra at three locations on a fresh mica disc: (a) at the plasma jet centre; (b) at a mid-point at 3 mm from the plasma centre and at the edge of the mica disc.

amyloid aggregates over a sustained period of time. The discontinuous sections seen in the mid-point image suggest a gradual fragmentation of fibrils, and may be indicative of structural changes that will require further investigation in the future.

It is useful to discuss potential plasma agents particularly reactive oxygen species that may have impacted on the samples at the mid-point and near the sample edge. Considerable reduction of amyloid aggregates was achieved in these remote areas, for which there were no substantial physical forces, for example plasma-assisted gas flow, surface tension due to charged particles, or even impact of fast-moving plasma bullets [63]–[65]. Figure 6 shows optical emission spectra obtained from three locations on a fresh mica surface, where several helium lines are evident at 501.6 nm ($3^1P \rightarrow 2^1S$), 587.6 nm ($3^3D \rightarrow 2^3P$), 667.8 nm ($3^1D \rightarrow 2^1P$), 706.5 nm ($3^3S \rightarrow 2^3P$), and 728.1 nm ($3^1S \rightarrow 2^1P$) as well as the two excited atomic oxygen lines at 777.3 nm (3^5P–3^5S) and 844.6 nm (3^3P–3^3S). Also found are nitrogen lines, for example the first negative system ($B^2\Sigma_u^+ \rightarrow X^2\Sigma_g^+$) of N_2^+ ions at 391.4 and 427.8 nm for the (0,0) and (0,1) band, respectively, and the N_2 line second positive system below 380 nm ($C^3\Pi_u \rightarrow B^3\Pi_g$). These emission lines become much smaller at the mid-point of the mica disc sample and its edge, but the proportional reduction is the smallest for the two excited atomic oxygen lines and even at the edge of the mica disc the 777 nm line remains distinct. UV emission was also estimated using an UVX radiometer and a short-wavelength sensor covering 250–290 nm (UV Process Supply Inc, Chicago, USA). With the radiometer used as the substrate to the plasma plume, the wavelength-integrated emission was found to be well below 1 μW cm^{-2} outside the plasma diameter. This is much smaller than the necessary level of UV flux for protein damage [66]. Therefore the amyloid reductions observed were probably caused by neutral reactive plasma species rather than UV photons and charged particles. These neutral species include excited oxygen atoms and possibly also ground-state oxygen atoms and ozone, though direct concentration measurement of the latter is beyond the scope of this paper. Their delivery to the remote sample areas were likely by means of radial diffusion and/or advection, with an glancing effect rather than a head-on impact. In other words, physical removal was unlikely to

have contributed to the reduction of amyloid aggregates in areas outside the plasma diameter. It could be suggested that the glancing action may result in diffusion of reactive oxygen species into the porous structure of the amyloid aggregates, thus oxidizing parts of the fibrils in their diffusion path and resulting in a 'skeleton' of reduced aggregates on the sample surface where the original aggregates perhaps stacked the most. Since this impact is chemical rather than physical, the skeleton structure is likely to be littered with fibrils fragments that are likely to have only a loose adherence to the mica surface. This view is supported by the fact that the image of the skeleton structure of figure 5 has a blurry boundary and that physical forces of detachment would have removed the fragmented fibrils to leave a distinctly resolved image.

The above discussion suggests a high likelihood that amyloid aggregates outside the plasma region were reduced through degradation, possibly initiated by oxidation, with only little contribution from peeling-off forces and other physical effects. At the sample centre where the plasma jet impacted directly, the reduction of amyloid aggregates is much more significant. This could be due to either a more aggressive oxidation effect, or additional physical impact, or their combined synergistic effects. From our current AFM data, the possibility of physical peel-off effects cannot be ruled out. However, the comparison of the three cases with 2 s plasma treatment in figure 5 suggests that it is certainly possible with CAPs to achieve degradation of amyloid aggregates, and probably other proteins with a cross-β structure including prions. This will need to be confirmed by structural studies using, for example, solid-state Nuclear Magnetic Resonance (NMR), and is outside the scope of this paper. In the context of prion inactivation, it is possible to configure plasma–sample interactions so as to minimize and eliminate the possibility of the physical detachment of amyloid aggregates. This is important because a process that relies on physical removal could result in an undesirable physical transfer of prion contaminants from one location to another.

Figure 7 shows AFM images of amyloid aggregates after longer plasma treatment times up to 8 s. Again in the central regions, plasma treatment left little on the mica surface but some scattered spherical objects of sub-micrometer sizes. For the mid-point images, the 2 and 4 s cases each have a cluster of bright-looking fibrils that appear to be stacked whereas the 6 and 8 s cases appear to have more flattened layers of fibrils. This is suggestive of a progressive reduction of the aggregates. Fibril fragmentation is evident in all cases, even in the 2 and 4 s cases where fibril stacking appears to be significant. A greater extent of fragmentation is seen in the 6 s case with many finer-sized objects. Near the sample edge, the results show a similarly progressive reduction, although the 8 s image appears to show more stacking. This could be due to spatial variation of the original amyloid aggregate sample on its mica disc, variation in spatial distributions of different plasma species under environmental interference, or time-dependence of different neutral plasma species in space. In general, figure 7 adds further evidence to that shown in figure 5 that neutral plasma species particularly reactive oxygen species could be facilitated to diffuse into the porous structure of amyloid aggregates and that this plasma action is likely to degrade the amyloid fibrils, potentially disturbing their structures and hence modifying their functions such as infectivity. This is an important subject of research for future studies.

Although direct biological and structural evidence may be considered as the ultimate confirmation of the degrading action of CAP, such work requires a substantial investigation well outside the scope of this work. Here, we chose instead to employ XPS to establish whether elemental compositions may have been altered by the impact of CAPs. In our discussion of figure 5, reduction of amyloid aggregates away from the plasma jet is attributed to neutral

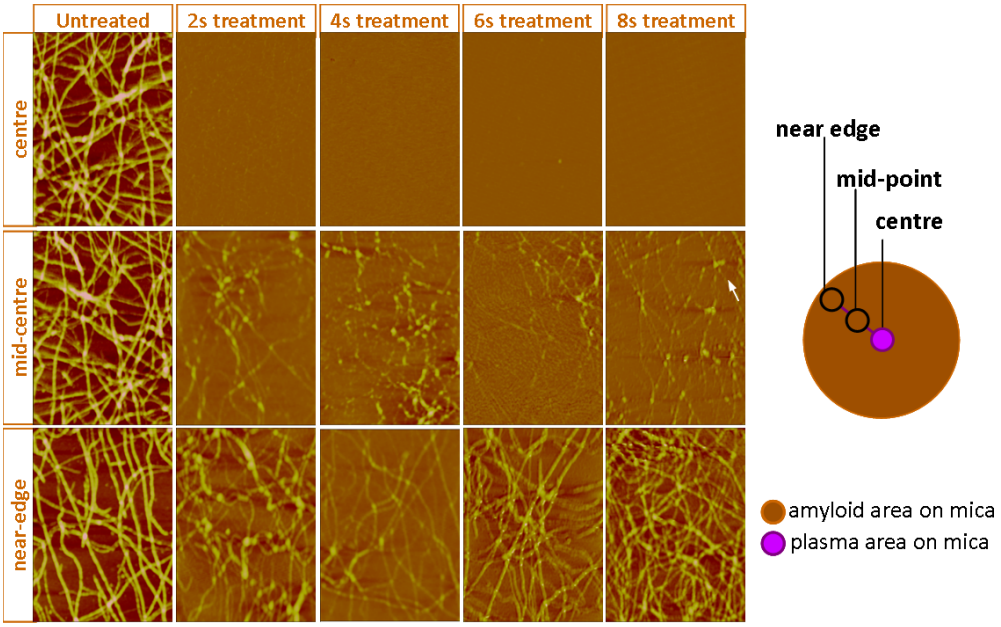

Figure 7. AFM images of amyloid aggregates obtained at the sample centre (the first row), near the mid-point along a radial line between the centre and the sample edge (the second row) and near the sample edge (the third row). The schematic on the right indicates plasma diameter of ∼2 mm in relation to the sample diameter of 9.9 mm. Images in the first are control and the remaining columns are treatments for 2, 4, 6 and 8 s.

species and their oxidation whereas that impacted directly by the plasma jet could potentially include both oxidation and physical removal. We therefore performed XPS analysis of untreated amyloid sample, the central area of a treated sample and a remote area 3 mm from the centre of the treated sample. In analysing compositions of different bonds, we considered the contribution of clean mica discs which already had C–C bonds present. In order to see if there were any changes in the proportions of different chemical bonds, contributions resulting from the C–C bonds in the underlying clean mica must be removed. This was achieved by (i) using the K (2p) peak next to the C peak for a clean mica disc, (ii) using their ratio and the K peak detected for an amyloid sample to deduce C–C bond contribution of the mica disc itself to the amyloid sample, finally (iii) obtaining C–C bond contribution from the amyloid aggregates by taking away C–C bond contributions of the underlying mica disc. Peaks of various chemical bonds were estimated using a peak fitting software used routinely for the XPS system. The procedure described above to remove contributions of the underlying mica disc to XPS signals made the data more reliable.

Figure 8 shows XPS analysis data for untreated and treated mica disc (figures 8(a) and (b)), and for an untreated amyloid sample and a plasma treated amyloid sample with the latter for a remote area at 3 mm from the plasma contact point on the sample surface (figures 8(c) and (d)). The two mica samples (without amyloid) show both C–C and Si–C bonds (figures 8(a) and (b)). The plasma-treated amyloid sample (figure 8(d)) had an additional Si–C peak from the underlying mica disc, whose signal was reduced by the overlying amyloid aggregates to below their detection limit in the untreated amyloid sample (figure 8(c)). Therefore the overall curve shape in figure 8(d) is distorted by the Si–C peak. However, a careful examination of the other

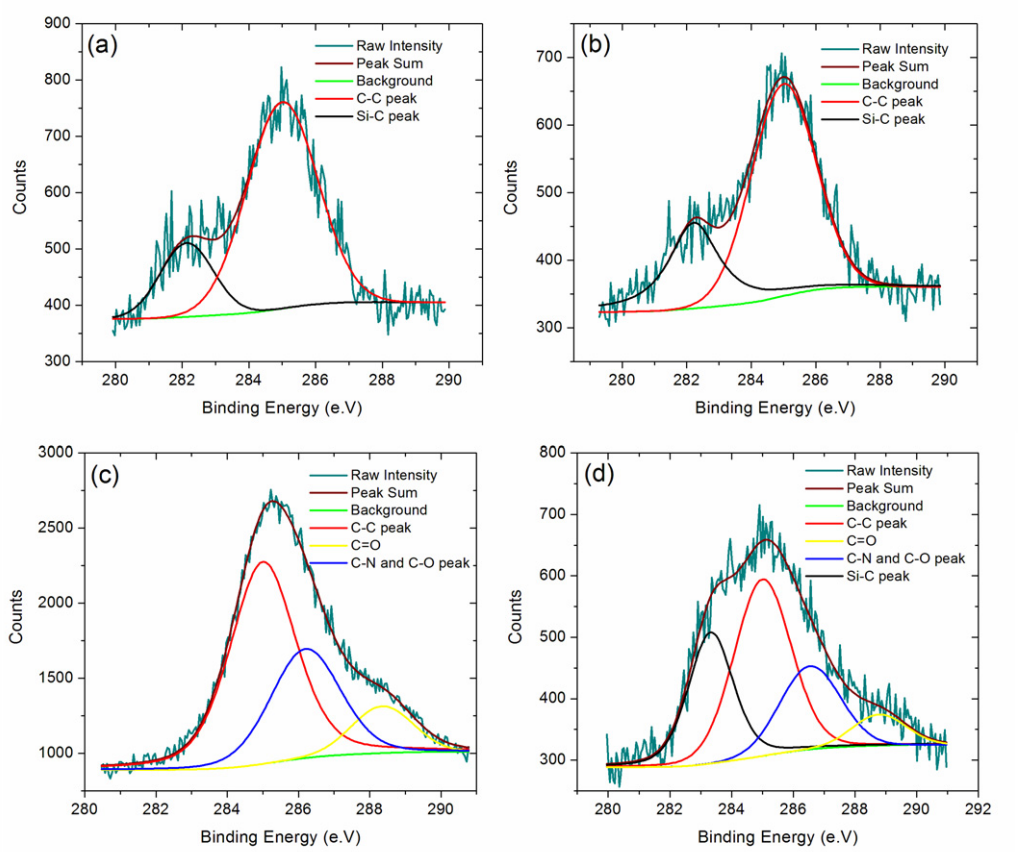

Figure 8. XPS analysis of (a) an untreated mica sample; (b) a treated mica sample (2 s); (c) an untreated amyloid sample and (d) a CAP-treated plasma sample with 2 s treatment and sampled at 3 mm from the sample centre.

four peaks, namely C–C, C = O and combined C–N/C–O bonds, revealed marked changes. To see this clearly, percentage distributions of the three bonds are shown in table 1 for (i) the untreated amyloid sample; (ii) the central area of a treated amyloid sample (impacted directly by the light-emitting part of the plasma jet); and (iii) a remote area of the treated amyloid sample at 3 mm from the sample centre. Plasma treatment time was 2 s under identical conditions to those for the last column in figure 5. It is clear from table 1 that the percentage distribution of the four chemical bonds remained roughly the same for the untreated amyloid sample and the central area of the treated sample. By contrast, the remote areas of the treated amyloid sample show distinct deviation in the distribution of different bonds to that of the untreated sample. This strongly suggests that direct plasma impact (to the central area) is likely to be dominated by a physical removal, perhaps accompanied by damage due to reactive oxygen species. However, the indirect plasma impact to sample areas remote from the light-emitting part of the plasma jet altered the chemical make up of the intact amyloid aggregates. In other words, amyloid aggregates in remote areas of the surface were most likely to have suffered degradation. This is consistent with the conclusions from the AFM data in figures 5 and 6.

The rapid removal of amyloid aggregates by direct plasma impact over a short duration of 2 s suggests a significant role of physical removal. This physical removal can be mitigated by

Table 1. Different chemical bonds in CAP treated and untreated amyloid aggregates.

		Treated amyloid sample at	
	Untreated amyloid (%)	Sample centre (%)	3 mm from centre (%)
C═O	13.13	13.10	13.86
C–N + C–O	37.53	38.02	42.05
C—C	49.34	48.87	44.09

reducing the plasma dosage so that reactive plasma species are allowed to work on amyloid aggregates. The spatial profile of the plasma action can be mitigated by using a CAP jet array [48, 67], and this will be investigated in future work. In principle, it is possible to tailor plasma conditions specifically to promote protein degradation and eliminate physical protein removal. It is worth mentioning that the small spherical fragments visible in the images of the first row of figure 7 were found to produce small nitrogen peaks close to the XPS detection limit. These could be traces of proteinaceous matter left over following plasma treatment or alternatively, of nitrogen introduced into the mica surface by the plasma treatment. In fact, XPS results on clean mica showed nitrogen being introduced onto the surface (data not shown). This is possible because of the interaction between the helium CAP jet and the nitrogen in the ambient air. Results from AFM and XPS for amyloid aggregates are encouraging, and if they could be reproduced for prions it would offer a real hope for plasma-enabled control strategy to combat prion infectivity.

4. Conclusions

As a non-infectious prion model, amyloid protein having a cross-β structure was deposited on freshly cleaved mica disc and grown into aggregates of mature fibrils for gas plasma treatment. A CAP jet was generated in helium–oxygen flow with 0.5% oxygen admixture, and a pulsed RF excitation was used to maintain the gas temperature at around 37 °C and facilitate non-thermal degradation of amyloid aggregates. At an input RF power at 4 W and in only 2 s of plasma treatment, very significant reduction of amyloid aggregates was achieved on sample areas that were directly treated by the plasma jet. Considerable amyloid reduction was also achieved in areas of the sample that were distant from the light-emitting part of the plasma, and the reduction led to the formation of a skeleton of reduced aggregate stacks with fragmented fibrils. Significantly, because the skeleton structure was observed outside the plasma jet region, and so was not subject to any physical forces of detachment, amyloid degradation was likely to have occurred predominately by a progressive diffusion of oxidizing neutral plasma species into the porous aggregate structure. The level of aggregate reduction and fibril fragmentation was most likely achieved as a result of reaction chemistry of neutral plasma species particularly oxygen atoms and ozone. This suggests the possibility of on-site degradation by CAP treatment with little possibility of physical removal, thus offering a new fundamental capability with desirable implications for practical implementation of CAP-based sterilization systems. Additional XPS data revealed that the effect of CAP jets was largely degradation in remote sample areas

outside the plasma diameter, but the area within the plasma diameter sustained largely physical removal of amyloid aggregates. While it would be desirable to follow up this work with amyloid structural studies, the results presented here already support strongly the viability of CAP-based degradation of proteins with cross-β structures possibly even prions.

References

[1] Laroussi M 1996 *IEEE Trans. Plasma Sci.* **24** 1188
[2] Moisan M, Barbeau J, Moreau S, Pelletier J, Tabrizian M and Yahia L H 2001 *Int. J. Pharm.* **226** 1
[3] Deng X T, Shi J and Kong M G 2006 *IEEE Trans. Plasma Sci.* **34** 1310
[4] Perni S, Shama G, Hobman L, Lund P A, Kershaw C J, Hidalgo-Arroyo G A, Penn C W, Deng X T, Walsh J L and Kong M G 2007 *Appl. Phys. Lett.* **90** 073902
[5] Fridman G, Friedman G, Gutsol A, Shekhter A B, Vasilets V N and Fridman A 2008 *Plasma Process Polym.* **5** 503
[6] Morfill G E 2009 The Munich plasma medicine project: results and current status Presented at *2nd Int. Conf. Plasma Medicine (San Antonio/TX USA, 16–20 March 2009)*
[7] Stoffels E, Flikweert A J, Stoffels W W and Kroesen G M W 2002 *Plasma Sources Sci. Technol.* **11** 383
[8] Fridman G, Shereshevsky A, Jost M M, Brooks A D, Fridman A, Gutsol A, Vasilets V and Friedman G 2007 *Plasma Chem. Plasma Process.* **27** 163
[9] Kim G C, Kim G J, Park S R, Jeon S M, Seo S J, Iza F and Lee J K 2009 *J. Phys. D: Appl. Phys.* **42** 032005
[10] Lee H J, Shon C H, Kim Y S, Kim S, Kim G C and Kong M G 2009 *New J. Phys.* **11** 115026
[11] Stoffels E 2007 *Contrib. Plasma Phys.* **47** 40
[12] Lu X P, Cao Y G, Yang P, Xiong Q, Xiong Z L, Xian Y B and Pan Y 2009 *IEEE Trans. Plasma Sci.* **37** 668
[13] Lee H W, Kim G J, Kim J M, Park J K, Lee J K and Kim G C 2009 *J. Endod.* **35** 587
[14] Jiang C, Chen M T, Schaudinn C, Gorur A, Vernier P T, Costerton J W, Jaramillo D E, Sedghizadeh P P and Gundersen M A 2009 *IEEE Trans. Plasma Sci.* **37** 1190
[15] Deng S, Ruan R, Mok C K, Huang G, Lin X and Chen P 2007 *J. Food Sci.* **72** M62
[16] Perni S, Liu D W, Shama G and Kong M G 2008 *J. Food Protect.* **71** 302
[17] Perni S, Shama G and Kong M G 2008 *J. Food Protect.* **71** 1619
[18] Selcuk M, Oksuz L and Basaran P 2008 *Bioresour. Technol.* **99** 5104
[19] Akitsu T, Ohkawa H, Tsuji M, Kimura H and Kogoma M 2005 *Surf. Coating Technol.* **191** 29
[20] Vleugels M, Shama G, Deng X T, Greenacre E, Brocklehurst T and Kong M G 2005 *IEEE Trans. Plasma Sci.* **33** 824
[21] Rahul R, Stan O, Rahman A, Littlefield E, Hoshimiya K, Yalin A P, Sharma A, Pruden A, Moore C A, Yu Z and Collins G J 2005 *J. Phys. D: Appl. Phys.* **38** 1750
[22] Laroussi M, Tendero C, Lu X, Alla S and Haynes W L 2006 *Plasma Process Polym.* **3** 470
[23] Sato T, Miyahara T, Doi A and Ochiai S 2006 *Appl. Phys. Lett.* **89** 073902
[24] Yu H, Perni S, Shi J J, Wang D Z, Kong M G and Shama G 2006 *J. Appl. Microbiol.* **101** 1323
[25] Sladek R E J, Filoche S K, Sissons C H and Stoffels E 2007 *Lett. Appl. Microbiol.* **45** 318
[26] Opretzka J, Benedikt J, Awakowicz P, Wunderlich J and von Keudell A 2007 *J. Phys. D: Appl. Phys.* **40** 2826
[27] Brandenburg R, Ehlbeck J, Stieber M, von Woedtke T, Zeymer J, Schluter O and Weltmann K D 2007 *Contrib. Plasma Phys.* **47** 72
[28] Fridman G, Brooks A D and Balasubramanian M 2007 *Plasma Process Polym.* **4** 370
[29] Vandervoort K G, Abramzon N and Brelles-Marino G 2008 *IEEE Trans. Plasma Sci.* **36** 1296
[30] Li G, Li H P, Wang L Y, Wang S, Zhao H Y, Sun W T, Xing X H and Bao C Y 2008 *Appl. Phys. Lett.* **92** 221504
[31] Gweon B, Kim D B, Moon S Y and Choe W 2009 *Curr. Appl. Phys.* **9** 625
[32] Lemmer K, Mielke M, Pauli G and Beekes M 2004 *J. Gen. Virol.* **85** 3805
[33] Rutala W A and Weber D J 2001 *Clin. Infect. Dis.* **32** 1348

[34] Prusiner S B 1998 *Proc. Natl Acad. Sci. USA* **95** 13363
[35] Weissmann C, Enari M, Klöhn P C, Rossi D and Flechsig E 2002 *J. Infect. Dis.* **186** S157
[36] Baxter H C, Campbell G A, Whittaker A G, Jones A C, Aitken A, Simpson A H, Casey M, Bountiff L, Gibbard L and Baxter R L 2005 *J. Gen. Virol.* **86** 2393
[37] Baxter H C, Campbell G A, Richardson P R, Jones A C, Whittle I R, Casey M, Whittaker A G and Baxter R L 2006 *IEEE Trans. Plasma Sci.* **34** 1337
[38] Bernard C, Leduc A, Barbeau J, Saoudi B, Yahia L H and De Crescenzo G 2006 *J. Phys. D: Appl. Phys.* **39** 3470
[39] Kylian O, Rauscher H, Gilliland D, Bretagnol F and Rossi F 2008 *J. Phys. D: Appl. Phys.* **41** 095201
[40] Rogez-Kreuz C *et al* 2009 *Infect. Control Hosp. Epidemiol.* **30** 769
[41] Deng X T, Shi J J, Chen H L and Kong M G 2007 *Appl. Phys. Lett.* **90** 013903
[42] Deng X T, Shi J J and Kong M G 2007 *J. Appl. Phys.* **101** 074701
[43] Giles K, Glidden D V, Beckwith R, Seoanes R, Peretz D, DeArmond S J and Prusiner S B 2008 *PLoS Pathogens* **4** e1000206
[44] Nelson R, Sawaya M R, Balbirnie M, Madsen A Ø, Riekel C, Grothe R and Eisenberg D 2005 *Nature* **435** 773
[45] Fändrich M and Dobson C M 2002 *EMBO J.* **21** 5682
[46] Walsh J L, Shi J J and Kong M G 2008 *Appl. Phys. Lett.* **88** 171501
[47] Hubicka Z, Cada M, Sicha M, Churpita A, Pokorny P, Soukup L, and and Jastrabik L 2002 *Plasma Source Sci. Technol.* **11** 195
[48] Cao Z, Walsh J L and Kong M G 2009 *Appl. Phys. Lett.* **94** 021501
[49] Walsh J L and Kong M G 2008 *Appl. Phys. Lett.* **93** 111501
[50] Deng X T, Shi J, Shama G and Kong M G 2005 *Appl. Phys. Lett.* **87** 153901
[51] Deng X T and Kong M G 2004 *IEEE Trans. Plasma Sci.* **32** 1709
[52] Shi J J and Kong M G 2005 *Appl. Phys. Lett.* **87** 201501
[53] Moon S Y, Kim D B, Gweon B and Choe W 2008 *Appl. Phys. Lett.* **93** 221506
[54] Brandenburg R, Ehlbeck J, Stieber M, Woedtke T V, Zeymer J, Schlüter O and Weltmann K D 2007 *Contrib. Plasma Phys.* **47** 72
[55] Walsh J L, Iza F and Kong M G 2008 *Appl. Phys. Lett.* **93** 251502
[56] Ye R, Ishigaki T and Sakuta T 2005 *Plasma Sources Sci. Technol.* **14** 387
[57] Leveille V and Coulombe S 2005 *Plasma Sources Sci. Technol.* **14** 467
[58] Balcon N, Aanesland A and Boswell R 2007 *Plasma Sources Sci. Technol.* **16** 217
[59] Shi J J, Zhang J, Qiu G, Walsh J L and Kong M G 2008 *Appl. Phys. Lett.* **93** 041502
[60] Stine W B Jr, Dahlgren K N, Krafft G A and LaDu M J 2003 *J. Biol. Chem.* **278** 11612
[61] Moravej M, Babayan S E, Yang X, Nowling G R and Hicks R F 2004 *J. Appl. Phys.* **96** 7011
[62] Giurleo J T, He X and Talaga D S 2008 *J. Mol. Biol.* **381** 1332
[63] Teschke M, Kedzierski J, Finantu-Dinu E G, Korzec D and Engemann J 2005 *IEEE Trans. Plasma Sci.* **33** 310
[64] Lu X and Laroussi M 2006 *J. Appl. Phys.* **100** 063302
[65] Shi J, Zhong F, Zhang J, Liu D W and Kong M G 2008 *Phys. Plasmas* **15** 013504
[66] Thakur A K and Rao C M 2008 *PLoS One* **3** e2688
[67] Nie Q, Zao Z, Ren C S, Wang D Z and Kong M G 2009 *New J. Phys.* **11** 115015